


## Article

# Optimization of Selective Laser Sintering/Melting Operations by Using a Virus-Evolutionary Genetic Algorithm

Nikolaos A. Fountas <sup>1</sup>, John D. Kechagias <sup>2</sup> and Nikolaos M. Vaxevanidis <sup>1,\*</sup>

<sup>1</sup> Department of Mechanical Engineering, School of Pedagogical and Technological Education (ASPETE), GR 151 22 Amarousion, Greece

<sup>2</sup> Design & Manufacturing Lab (DML), Department of FWSD, University of Thessaly, 43100 Karditsa, Greece

\* Correspondence: vaxev@aspete.gr; Tel.: +30-210-2896841

**Abstract:** This work presents the multi-objective optimization results of three experimental cases involving the laser sintering/melting operation and obtained by a virus evolutionary genetic algorithm. From these three experimental cases, the first one is formulated as a single-objective optimization problem aimed at maximizing the density of Ti6Al4V specimens, with layer thickness, linear energy density, hatching space and scanning strategy as the independent process parameters. The second one refers to the formulation of a two-objective optimization problem aimed at maximizing both the hardness and tensile strength of Ti6Al4V samples, with laser power, scanning speed, hatch spacing, scan pattern angle and heat treatment temperature as the independent process parameters. Finally, the third case deals with the formulation of a three-objective optimization problem aimed at minimizing mean surface roughness, while maximizing the density and hardness of laser-melted L316 stainless steel powder. The results obtained by the proposed algorithm are statistically compared to those obtained by the Greywolf (GWO), Multi-verse (MVO), Antlion (ALO), and dragonfly (DA) algorithms. Algorithm-specific parameters for all the algorithms including those of the virus-evolutionary genetic algorithm were examined by performing systematic response surface experiments to find the beneficial settings and perform comparisons under equal terms. The results have shown that the virus-evolutionary genetic algorithm is superior to the heuristics that were tested, at least on the basis of evaluating regression models as fitness functions.

**Keywords:** virus-evolutionary genetic algorithm; optimization; selective laser sintering; heuristics; additive manufacturing; hardness; density; tensile strength



**Citation:** Fountas, N.A.; Kechagias, J.D.; Vaxevanidis, N.M. Optimization of Selective Laser Sintering/Melting Operations by Using a Virus-Evolutionary Genetic Algorithm. *Machines* **2023**, *11*, 95. <https://doi.org/10.3390/machines11010095>

Academic Editor: António Bastos Pereira

Received: 26 November 2022

Revised: 5 January 2023

Accepted: 9 January 2023

Published: 11 January 2023



**Copyright:** © 2023 by the authors. Licensee MDPI, Basel, Switzerland. This article is an open access article distributed under the terms and conditions of the Creative Commons Attribution (CC BY) license (<https://creativecommons.org/licenses/by/4.0/>).

## 1. Introduction

Setting advantageous values for the process parameters in manufacturing processes constitutes a crucial task in process planning, requiring extensive experience in manufacturing engineering operations, deep knowledge of establishing and conducting systematic experiments, a mathematical background concerning the statistical analysis of experimental results and comprehensive know-how for formulating machining modeling problems for optimization [1–4]. Unfortunately, such elements can hardly be implemented in real-world applications owing to the tedious efforts of process planners under pressing timespans and high productivity/quality requirements. Consequently, industrial practices still suggest the usage of handbooks, manuscripts and tool catalogues in order to examine the operational ranges for different process parameters which try to determine advantageous—if not optimal—settings for them as a combination of parameter values that will affect the whole process. This approach continues to be applied since systematic experimentation and parameter examination are time-consuming processes that also contribute to higher costs.

To set an “optimum” combination for the parameter values, several researchers have developed and implemented various algorithmic modules following the principles of dynamic programming [5,6], goal programming [7], integer linear programming [8] and

fuzzy environments [9]. Even though such systems have succeeded in solving several engineering optimization problems, they come with certain drawbacks in regards to their objective-dependent searching mechanisms, as well as their constraint-type functions (i.e., non-linear and/or linear ones). In addition, they are unable to maintain the same efficiency when they are altering the size of the solution domain or its structure (i.e., convex, concave and saddle ones, etc.).

To solve the numerous engineering optimization problems with the highest rate of success, researchers have proposed the implementation of algorithms that adhere to either population or swarm intelligence. In the work presented in [10], the authors took advantage of an optimization problem related to the abrasive water jet machining, which was originally studied in [11]. In their work, they implemented the Greywolf algorithm [12] to maximize the material removal rate (*MRR*), with the nozzle diameter, the feed of nozzle, the mass flow rate of the abrasives, the water mass flow rate and the water pressure at the nozzle as the independent process parameters. In the same work presented in [10], a second case was solved by the Greywolf algorithm related to a bi-objective problem that was originally examined in [13]. In this case, the objectives of *MRR* and *Ra* were simultaneously optimized, exhibiting their trade-off, owing to *MRR* maximization and *Ra* minimization requirement. The authors in [14] implemented their Teaching/Learning optimization algorithm (TLBO) to solve three non-conventional machining processes based on previous experimental works conducted by others, namely, ultrasonic machining (USM), abrasive jet machining (AJM) and wire electro-discharge machining (wEDM). The TLBO algorithm was also applied in [15] to solve three single-objective and two multi-objective problems concerning fused deposition modeling (FDM). All five case studies reported in this work were based on previous experimental works [16–20]. Under the same research concept, the authors of [21] implemented the MO-Jaya algorithm to optimize the previously investigated machining operations; wire electro-discharge machining [22], the laser cutting process [23], electrochemical machining [24] and focused ion beam (FIB) micro-milling [25]. Other machining and micro-machining processes based on the experiments of others were also optimized using the TLBO algorithm [26], while some other abrasive waterjet machining operations were optimized using the Jaya algorithm along with the PROMETHEE method [27].

The initial variant of the virus-evolutionary genetic algorithm (VEGA) was developed and implemented in several research works with emphasis to those that are presented in [28] and [29]. An enhanced version of this algorithm was later proposed in [30]. A noticeable characteristic of the original variant of the VEGA was the transformation of the multi-objective optimization problems to single-objective ones through the adaptation of the “weighted summation” strategy [31].

This paper implements a virus-evolutionary genetic algorithm that is capable of controlling both the techniques for solving optimization problems (single and multi-objective ones). To enable this control, a sub-routine that activates the functions related to single or multi criteria processing has been programmed. Emphasis is given to the multi-objective optimization selection, where a single simulation run can prompt the algorithm to evaluate an entire set comprising many non-dominated solutions existing in a Pareto front. In the case of a multi-objective problem represented by using the “weighted summation” approach, the proposed virus-evolutionary genetic algorithm investigates the problem with the determination of all the possible combinations among the weights applied to the objectives. The multi-objective virus-evolutionary genetic algorithm is called MOVEGA in the paper. The MOVEGA is applied to solve three problems related to a cutting-edge additive manufacturing process that is widely known as selective laser sintering—selective laser melting (SLS-SLM). All the problems have been formulated with reference to the regression equations that are derived from original experiments, and they are quadratic and parameter bounded. In the first case, the processing layer thickness, linear energy density, hatching space and scanning strategy are treated as the independent process parameters, with the maximum density of the manufactured specimens being the objective of interest.

The second case uses the laser power, scanning speed, hatch spacing, scan pattern angle and heat treatment temperature as the independent variables, while maximum hardness and maximum tensile strength are considered as the optimization objectives. Finally, the third case presents a three-objective optimization problem where the laser power, scanning speed and hatch spacing are the independent variables, whilst the minimum mean surface roughness, maximum density and maximum hardness are treated as the optimization objectives. The regression models used for optimizing the aforementioned problems have been previously validated with regard to the corresponding experiments conducted by previous researchers.

## 2. Virus-Evolutionary Genetic Algorithm for Multi-Objective Optimization (MOVEGA)

Two methods are distinguished for creating new candidate solutions to solve a combinatorial problem. The first method is based on a stochastic philosophy, whereas the second method is associated with local information that characterizes the problem. Even though genetic algorithms (GAs) are primarily considered as stochastic search modules, local information is very useful in order to escape from local optima and increase the possibility of finding the global optimum solution to a problem. Crossover and selection operators are used for creating new candidate solutions, and they provide local information for the search space. The mechanism of generating new effective individuals under the concept of producing robust schemata is prone to premature local convergence when one applies only a proportional selection. On the contrary, MOVEGA targets a promising substring from the binary encoded string of an individual and creates the virus individual. By combining the strings of the individuals and viruses, the algorithm manages to produce new candidate solutions in horizontal propagation. This strategy is quite promising since the coevolution among hosts and viruses (global and local information) facilitates fast optimization problem solving.

The virus theory of evolution suggests that virus transduction is of paramount importance for transporting genetic segments across species [32]. Transduction implies the genetic modification of a bacterium by the genes from another bacterium transported through a bacteriophage. The majority of the viruses found in nature may easily cross species barriers, and they are usually transferred directly from individuals of one phylum to another. This means that natural viruses may transfer their gene to the host populations in horizontal propagation. In addition, the viruses may be included into germ cells, and thus, transmitted from generation to generation, following vertical inheritance. As a result, this paper applies a virus-evolutionary genetic algorithm that implements two operators; one of them is used for simulating vertical inheritance, and the other one is used simulating horizontal propagation. Two populations are created and co-evolve in this algorithm: the host population (candidate solutions) and the virus population (substrings of the selected host individuals). Typical genetic operators (i.e., selection and crossover ones) are implemented for performing standard activities in genetic algorithms, whilst the viral infection operators, which are the “reverse transcription” and “transduction” ones, are applied to simulate the natural operations of viruses. Figure 1 illustrates the functions of the two operators for performing viral infection.

In the program developed to build the functions of the proposed algorithm,  $C_{Pop}^{init}$  is the initial chromosomes population;  $Var$  is an independent parameter;  $N_b^{Var}{}_{i,j}$  is the number of bits necessary for representing the accuracy of each parameter  $Var$  for the  $i_{th}$  chromosome of the  $j_{th}$  population;  $Lgth_i$  is the  $i_{th}$  length of the chromosome. By considering the independent parameter  $Var_i$ , along with its corresponding bound  $D_{Var_i} = [Ub_i, Lb_i]$  and the  $i_{th}$  chromosome length  $Lgth_i$ , the formula given in Equation (1) can be used for switching from binary to real encoding.

$$Var_i = Lb_i + fnc(BinStr) \times \frac{Ub_i - Lb_i}{2^{Lgth_i} - 1} \quad (1)$$

where  $Ub_i$  and  $Lb_i$  are the parameters' upper and lower bounds, respectively, whilst  $fnc(BinStr)$  denotes the function for returning the decimal values referring to binary encoding based on their accuracy. When it comes to algorithmic simulations, there is a low possibility that an already evaluated individual from a previous run might be selected again. To avoid possibly selecting an already evaluated individual, a routine has been developed based on flag statements either 0 (a new individual) or 1 (an already examined individual from previous runs) in the *Microsoft® Visual Basic® for Applications* environment. Objective function computation is conducted for all the candidates in a population. Thereby, the results are examined by the ranking function, which ranks them based on their objective scores. The ranking is sorted into ascending order. The fitness evaluation follows next, and it is applied to every individual in a population. Elite individuals are those having attained the lowest scores in the ranking operation. The individuals are finally stored along with their corresponding fitness scores in a file ("fitnessScores.dat"), and they are sorted into descending order.

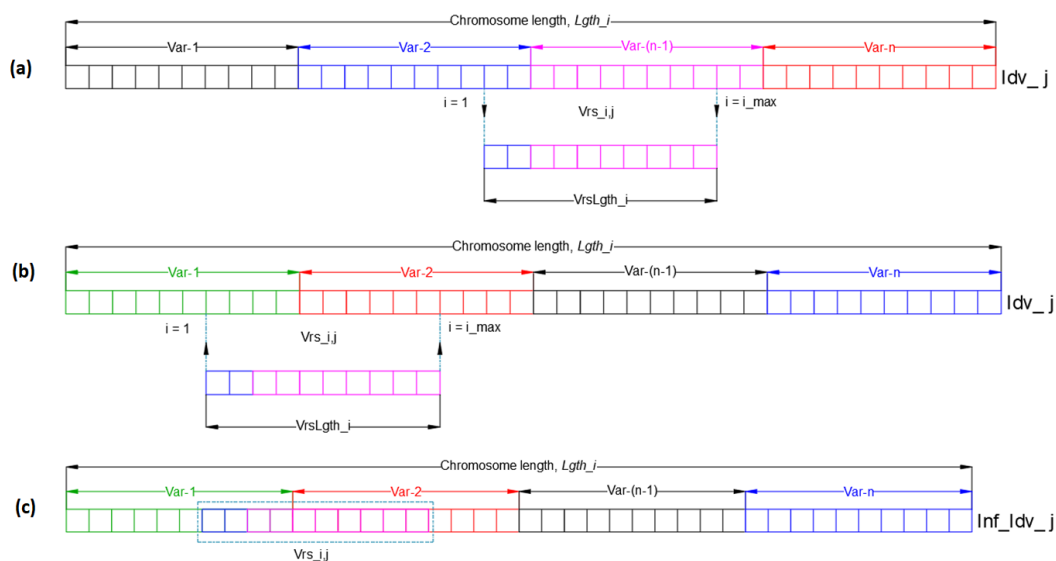


**Figure 1.** (a) Transduction operation for the generation of a virus individual. (b) Reverse transcription operation for infecting selected individuals with a virus. (c) Infected individual after the reverse transcription operation performed by a virus.

The process continues further by applying selection operator, where some individuals are selected for reproduction according to their fitness. Equation (2) represents the cumulative sum  $Fitsum$  of the entire population after importing the fitness scores of the individuals. The election range is formulated according to the lower and upper bounds, i.e., zero and  $Fitsum$ , respectively  $(0, Fitsum)$ . Further, the individuals are subsequently ranked with regard to their fitness score; i.e.,  $(0, Fit_1), (Fit_1, Fit_2), \dots, (Fit_{N-1}, Fitsum)$ , whereas a random generator is used to create the values within this region. The random generator produces as many random values as the number of selected individuals for the crossover. Random values exist between one of the above sub-ranges that denote the individuals that are to be selected. Thereby, elite individuals are favored according to their fitness so that the elitist behavior is maintained during the entire operation. After the selection of a particular individual is achieved, both the selection range  $[0, Fitsum]$  and the individual's sub-range are redefined by applying Equation (2) to prevent the iterative selection of this particular outstanding individual.

$$Fit_i = Fit_i - \frac{Fitsum}{2N} \tag{2}$$

where  $Fit_i$  is the fitness function score of  $i_{th}$  individual;  $N$  is the population's size;  $Fitsum$  is the aggregate sum of the entire population. The selected individuals are stored in a

dedicated file (“Selected.dat” file) to be further handled by the crossover operator. Pairs of individuals are randomly selected to produce offspring. When the crossover function is completed, all the individuals—the parents and offspring—are imported into a new candidate population (individual pool), whose size is twice as big as the initial population’s size. The objective function is computed again, and the individuals are ranked accordingly by applying a ranking function. Based on their ranking  $N$ , the best individuals are deterministically selected, where  $N$  is the original number of initial individuals that constitute the first population. Finally, the individuals are mutated to give a new population of candidate solutions.

The next operation is mutation. Mutation involves the number of individuals, the number of mutated variables in terms of binary digits (i.e., 0 and 1) and the mutation rate. A population—as a result of selection and crossover—is imported and processed in order to determine the pointers for the selected offspring to indicate the locations in chromosomes where the change between “0” and “1” digits are to be made. Mutation begins with a rather high initial probability to preserve the diversity of exploration, while it gradually lowers via a linear expression that involves the initial mutation rate value and the number of generations to prevent a completely scattered random search, thus, it has a high computational cost.

Viruses are created after the fitness evaluation of all the individuals comprising the main population is conducted. The number of viruses is actually a fraction of the main population’s magnitude. The MOVEGA algorithm manages to conduct both the targeted and random selection of individuals for infection. The former selection is applied to the elite of some outstanding individuals, whilst the latter one is normally applied to the rest individuals according to the probability. This ensures that there is an unbiased selection scheme. The successfully infected individuals appear as offspring. If their fitness score is improved after the infection, they replace their ancestors. Therefore, these individuals survive in the next generation. The initial chromosomes population  $C_{Pop}^{init}$  is randomly created, and then, a following transduction operation is applied to the fitted and randomly selected individuals for the creation of the virus population  $V_{Pop}^{init}$ . The viruses are stored in a binary representation of a related archive (“virus\_population.dat”). A single virus individual  $Vrs_{ij}$  is created by transducing from the  $i_{th}$  chromosome of the  $j_{th}$  population. The cut substrings represent the viruses’ chromosomes, whose length is  $VrsLgth_i$ .  $i = 1$  is the starting point from which the  $VrsLgth_i$  length is specified, while Locus  $i_{max}$  denotes the end point. These two points are randomly selected and constrained to the original host’s chromosome length  $Lgth_i$ . The chromosome length ( $Lgth_i$ ) of the individuals in the main population is constant, whereas the length of the virus individuals ( $VrsLgth_i$ ) increases as the evolution process continues ( $VrsLgth_i = V_{strlength} \max$ ). The population index from which selected individuals have been attacked is stored in the “infected\_host\_population.dat” archive. The phenotypes of the individuals that are candidates for infection are stored in the “virus\_phenotype.dat” archive. The objective results of the virus individuals are finally stored in the “virusobjvalues.dat” archive. Transduction and reverse transcription constitute the two fundamental operations of viral infection. The transduction operator is applied to the host individuals to generate the virus population. Viruses  $Vrs_{ij}$  attack to infect the individuals by applying reverse transcription to overwrite their own substrings to randomly selected segments of the individuals’  $Idv_j$  strings. The indices of  $Vrs_{ij}$  and  $Idv_j$  are “a priori” declared so as to perform the subsequent replacement of the binary digits according to the predetermined references.

An assessment of the virus individuals is achieved with the use of their fitness scores, which are denoted as  $FitVrs_{i,j}$ , reflecting their infection strength. This fitness is computed after the successful infection of  $Idv_j$  by  $Vrs_{ij}$ , as it is presented by Equation (3):

$$FitVrs_{i,j} = FitInfIdv_j - FitIdv_j \quad (3)$$

The value obtained by Equation (3) is the difference between the two fitness values of individual  $Idv_j$  before and after its infection by  $Vrs_{ij}$ . Given that  $Vrs_{ij}$  might infect more than a single individual (let  $S$  be the set of infected individuals),  $FitVrs_{i,j}$  reveals the improvement of fitness values of all the infected individuals, and as Equation (4) determines:

$$FitVrs_i = \sum_{j \in S} FitVrs_{i,j} \tag{4}$$

A virus  $Vrs_{ij}$  has a maximum viral infection rate  $V_{infRate}max$  for controlling the number of viral infections satisfying the relation  $1 \leq V_{infRate}max \leq 10$ . As a consequence, the number of reverse transcriptions that a single virus may perform will depend on its viral infection rate. The maximum viral infection rate  $V_{infRate}max$  is related also to its fitness value  $FitVrs_{i,j}$ . The higher the fitness  $FitVrs_{i,j}$  is, then the higher the  $V_{infRate}max$  will be. Equation (5) gives the relation adopted to relate the viral infection parameters mentioned above and control  $V_{infRate}max$  with regard to virus fitness  $FitVrs_{i,j}$ . In Equation (5),  $a (> 0)$  is a fixed parameter that is used to improve or degrade  $V_{infRate}max$  with regard to either the positive or negative results referring to virus fitness  $Vrs_{ij}$ .

$$V_{infRate}max_{i,G+1} = \begin{cases} (1 + a) \times V_{infRate}max_{i,G} & FitVrs_i \geq 0 \\ (1 - a) \times V_{infRate}max_{i,G} & FitVrs_i < 0 \end{cases} \tag{5}$$

A virus  $Vrs_{ij}$  has a life force indicator that represents its contribution to the main population in terms of its successful infections. The life force of a virus  $Vrs_{ij}$  is denoted as  $VrsLiforce_{i,G}$ , where  $i$  is the index of the virus  $Vrs_{ij}$  and  $G$  the current generation.  $VrsLiforce_{i,G}$  depends also upon the virus fitness  $Vrs_{ij}$ , and it is compared to the one obtained by the virus  $Vrs_{ij}$  in a previous generation. If its value is negative, then a new transduction operation is applied by the virus  $Vrs_{ij}$  to alter its scheme by randomly selecting an individual. Otherwise,  $Vrs_{ij}$  cuts a partially new substring by a successfully infecting an individual. The magnitude of  $VrsLiforce_{i,G}$  is computed in each generation according to the virus life reduction rate  $rate \downarrow V_{life}$ , satisfying  $0.001 \leq rate \downarrow V_{life} \leq 1.0$ . Therefore, the maximum viral infection rate  $V_{infRate}max$  and the virus life reduction rate  $rate \downarrow V_{life}$  are related through the expression given in Equation (6).

$$VrsLiforce_{i,G+1} = rate \downarrow V_{life} \times VrsLiforce_{i,G} + FitVrs_i \tag{6}$$

The  $V_{infRate}max$  and  $VrsLiforce_{i,G}$  parameters are initialized in MOVEGA as  $V_{infRate}max_{init} = V_{infRate}max_{i,0}$  and  $VrsLiforce_{i,0} = 0$ , respectively. The operation of partial transduction in the case where  $VrsLiforce_{i,G} < 0$  is presented in Figure 2 with reference to transduction and reverse transcription operations presented in Figure 1 above.

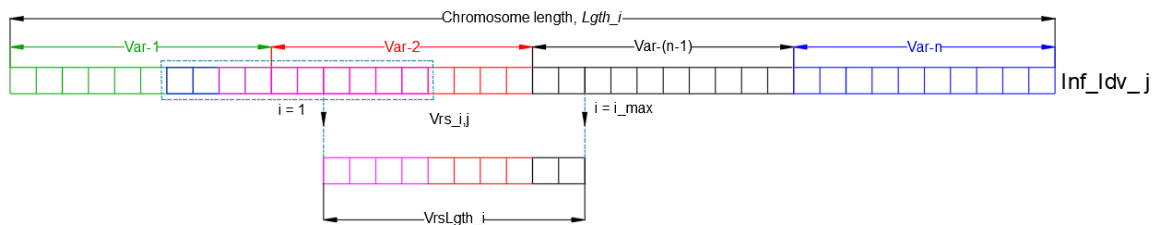


Figure 2. Partial transduction operation for changing the virus scheme.

The entire workflow (flow chart) for the proposed algorithm is presented in Figure 3.

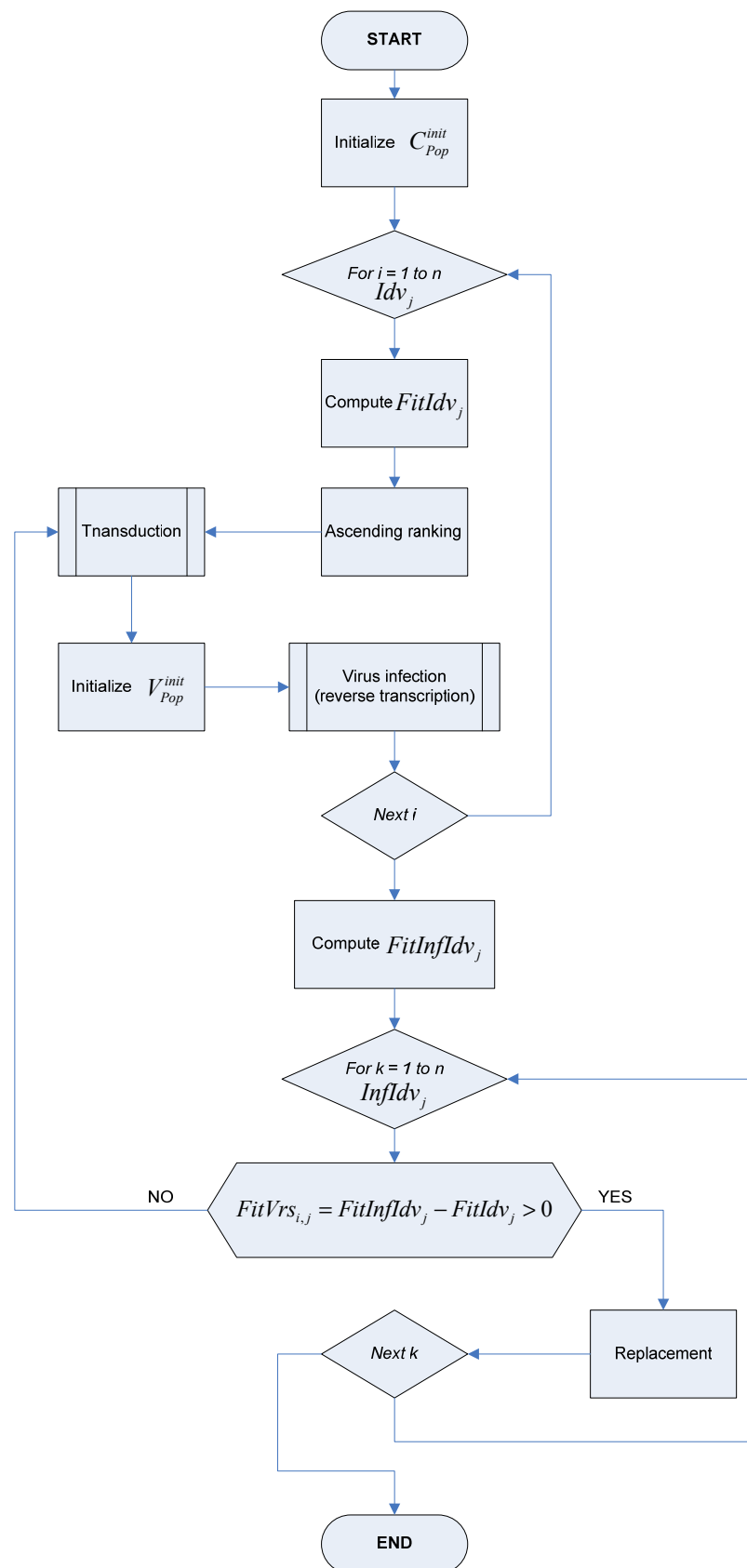


Figure 3. Flow chart of viral infection after the evaluation of main population’s individuals.

### 3. Performance Metrics

When it comes to multi-objective optimization, a diverse group of multiple non-dominated solutions are obtained. To examine and characterize the performance of an algorithm, some discrete performance metrics can be used. Two of the most important and commonly implemented metrics are the coverage of two sets  $Cvg(NDS_{i-1}, NDS_i)$  and the spacing  $S$  [33]. The coverage of two groups of non-dominated solutions ( $NDS_{i-1}, NDS_i$ ) refers to the percentage of dominance exhibited by the individuals of one group on the solutions of the other group. This metric can be computed by using the relation given in Equation (7).

$$Cvg(NDS_{i-1}, NDS_i) = \frac{|\{b \in NDS_i | \exists a \in NDS_{i-1} : a \leq b\}|}{|NDS_i|} \quad (7)$$

where  $NDS_{i-1}, NDS_i$  represent two non-dominated solution sets to compare;  $a \leq b$  implies that  $a$  either dominates it, or it is equal to  $b$ .  $Cvg(NDS_{i-1}, NDS_i) = 1$  implies that all the non-dominated solutions in  $NDS_i$  are dominated, or they are equal to all the non-dominated solutions in  $NDS_{i-1}$ , whilst  $Cvg(NDS_{i-1}, NDS_i) = 0$  implies that none of the non-dominated solutions of  $NDS_i$  are covered by those found in  $NDS_{i-1}$ . Note that both  $Cvg(NDS_{i-1}, NDS_i)$  and  $Cvg(NDS_i, NDS_{i-1})$  should be considered since there is a possibility that  $Cvg(NDS_{i-1}, NDS_i) \neq 1 - Cvg(NDS_i, NDS_{i-1})$ . In the case that  $Cvg(NDS_{i-1}, NDS_i) = 1$  and  $Cvg(NDS_i, NDS_{i-1}) = 0$ , the solutions of  $NDS_{i-1}$  entirely dominate those of  $NDS_i$ , and thus, this would be the ideal result for  $NDS_{i-1}$ . Thereby,  $Cvg(NDS_{i-1}, NDS_i)$  gives the percentage of the non-dominated points in  $NDS_i$  which are inferior or equal to the points in  $NDS_{i-1}$ , whereas  $Cvg(NDS_i, NDS_{i-1})$  gives the percentage of non-dominated points in  $NDS_{i-1}$  which are inferior or equal to the points in  $NDS_i$ .

Spacing is a performance metric used for quantifying the spread of the non-dominated solutions, or equivalently, how uniform the distribution among the different solutions is. The spacing metric is determined according to Equation (8) as follows:

$$S = \sqrt{\frac{1}{|n-1|} \sum_{i=1}^n (\bar{d} - d_i)^2} \quad (8)$$

In Equation (8),  $n$  is the number of the different non-dominated solutions in a Pareto front, whilst  $d_i = \min_{i, i \neq j} \sum_{Obj=1}^{ObjMax} |f_{Obj}^i - f_{Obj}^j|$ ,  $i, j = 1, 2, \dots, n$  is the distance variance.  $ObjMax$  is the maximum number of objectives,  $Obj$  is an objective number, and  $f_{Obj}$  is the objective function that corresponds to  $Obj$  objective. Since the objectives of interest might have different magnitudes, it is important to remove their inherent bias by normalizing them. Normalization can be achieved by using Equation (9).

$$\bar{d} = \sum_{i=1}^n \left( \frac{d_i}{|n|} \right) \quad (9)$$

In the case where  $S = 0$  (ideal and optimal case), all the non-dominated solutions are uniformly spread and equidistantly spaced to the entire Pareto front. The spacing indicator is suitable for evaluating the non-dominated solutions of the regular Pareto fronts, which are obtained by different algorithms. However, it is important that the solutions are unique, i.e., they cannot be duplicated.

### 4. Optimization Problems Related to Selective Laser Sintering/Melting—SLS/SLM

Selective laser sintering/melting (SLS/SLM) constitutes a very important, rapid prototyping process, where the materials in the form of powder are used for fabricating parts from computer-aided design (CAD) models. In the wide range of materials that are used for



SLS/SLM, one may distinguish engineering thermoplastics such as polymers, polyamides, ABS, nylons and polycarbonates, as well as metallic materials such as titanium and its alloys, stainless steel alloys and tool steels, etc. SLS/SLM is a very challenging operation owing to weak strength, dimensional inaccuracy and poor surface finish that characterize most of the products fabricated using SLS/SLM technology. As it occurs in any other manufacturing process, choosing the different settings for the values of process-related parameters is an important aspect. Since the problems presented in this research are examined in terms of optimization for the first time in the literature, no other reports were found to retrieve information about the algorithm-specific parameters and related settings. MOVEGA has been applied to solve all three problems with reference to preliminary research work concerning the tuning of the algorithm-specific parameters related to the proposed algorithm. Consequently, the settings applied for MOVEGA's parameters are ( $C_{pop} = 20$ ) for the population size, ( $V_{pop} = 12$ ) for the virus population size, the maximum variable number of bits in the virus chromosome substring, which is equal to 25 (given as a fraction of the 100-digit chromosome string of the individuals in the main population) ( $V_{strlengthmax} = 25 = \frac{1}{4}C_{strlengthmax}$ ), the maximum virus life reduction rate, which is equal to  $-0.5$  ( $rate \downarrow V_{life} = -0.5$ ), and the maximum infection rate, which is equal to 70% of the maximum viral infectivity ( $V_{infRatemax} = 7$ ). The same problems have been solved by applying other intelligent algorithms, with their algorithm-related parameters having been tuned to the best possible extend for rigorous comparisons to be made. These algorithms are mentioned in each problem, and they represent three population-based ones and one swarm-based one.

#### 4.1. Optimization of SLM Parameters for Forming Ti6Al4V Alloy Specimens with Maximum Density

The optimization procedure for the case study is based on the experimental results found in the work presented in [29]. In the aforementioned work, a custom SLM machine (DiMetal-280) was used for conducting the experiments. The major specifications of their machine are a continuous fiber laser with a wavelength of 1075 nm, the X-Y galvanometer scanning mode, which was focused by the  $f-\theta$  lens with a scanning velocity ranging from 5 to 5000 mm/s, the beam quality factor  $M^2 \leq 1.1$ , the laser spot diameter of 70  $\mu\text{m}$  and the thickness, which was layered by a roller and ranged from 20 to 80  $\mu\text{m}$ . The material was a gas-atomized spherical Ti6Al4V powder, while the average diameter of 95% powder was under 20  $\mu\text{m}$ . During the SLM operation, the oxygen content was below 0.02%. Based on the results in [29], a regression equation for estimating the mean density of produced parts was generated and adopted in this case for maximizing the mean density (%). However, the process parameters along with their corresponding ranges are the same as those considered by the authors of [29]. The parameters are: the processing layer thickness  $PT$  (mm), the linear energy density  $LED$  (J/mm) and the hatching space  $HS$  (mm). As a categorical factor, the scanning strategy was kept constant in the "X-Y inter-layer stagger scanning" mode. The ranges for the parameters were: ( $0.02 \leq PT \leq 0.035$ ), ( $0.2 \leq LED \leq 0.5$ ) and ( $0.04 \leq HS \leq 0.07$ ), according to [29]. Equation (10) gives the regression equation that was used as the objective function for maximizing the mean density  $\max\bar{\rho}$  in this single-optimization case.

$$\max\bar{\rho} = -\left(96.3 + 136 * PT + 13.1 * LED - 216 * HS - 630 * PT^2 - 46.4 * LED^2 - 1861 * HS^2 - 901 * PT * LED - 60 * PT * HS + 974 * LED * HS\right) \quad (10)$$

The authors of [29] optimized (maximized) the objective of the mean density  $\max\bar{\rho}$  by applying numerical optimization, and they achieved the value of 94.4424 (%) as the optimal solution. In [34] the optimal solution for the same problem was found equal to 94.4424. An attempt was conducted to further improve this result by applying the MOVEGA using its single-objective module. The same procedure was used for the rest of the optimizers used for comparison: the Greywolf algorithm (GWO), the Multiverse algorithm (MVO), the Antlion algorithm (ALO) and the Dragonfly algorithm (DA) [12,35–37]. The MOVEGA

as well as the competitive algorithms ran with a population size that was equal to 20 for 200 iterations, thus, resulting in 4000 function evaluations. All the algorithms managed to obtain the same maximum result for the mean density  $\max \bar{\rho}$ , which was equal to 94.4751 against the maximum value of 94.4424 reported in [34]. From the results obtained by the algorithms tested, in terms of the convergence speed and iteration number at which the best result was achieved, it is revealed that there is no need for setting such a large number of iterations, however, this has been intentionally considered in order to examine whether the algorithms become trapped in a local optimum solution or not. the MOVEGA (in this single-objective optimization case, it is referred as VEGA) exhibited the best convergence speed against the rest algorithms, whilst it obtained the maximum result for the mean density  $\max \bar{\rho}$  in the 6th iteration (120 function evaluations). The GWO, MVO, ALO and DA algorithms converged to the 17th, 53rd, 25th and 23rd iterations, respectively. The total execution timespan for the algorithms was approximately the same, ranging from 10 s to 13 s. Optimal values obtained were found that were equal to 0.02, 0.5 and 0.07 for the processing layer thickness  $PT$  (mm), linear energy density  $LED$  (J/mm) and hatching space  $HS$  (mm), respectively. These outputs are in full agreement with the experimental ones in [34]. Note that the algorithms were ran 20 times to examine their stochastic nature and repeatability for obtaining the best result. Figure 4 gives the best convergence trends exhibited by all the algorithms with regard to the total of 20 algorithmic simulation tests.

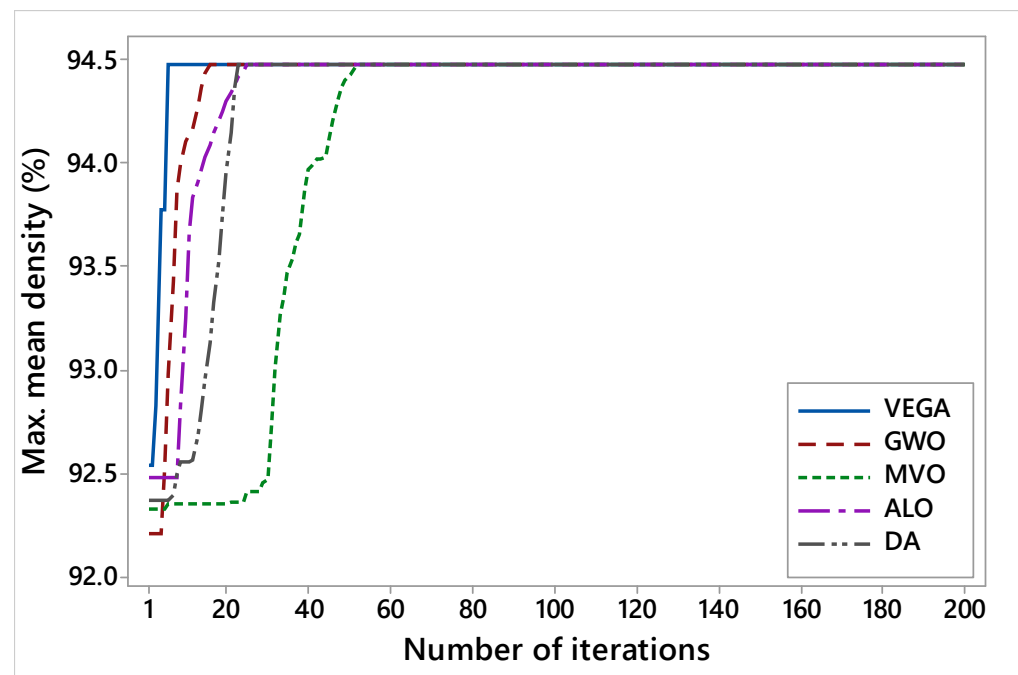


**Figure 4.** Convergence speed exhibited by VEGA, GWO, MVO, ALO and DA algorithms for maximizing mean density, with 200 iterations.

#### 4.2. Case 2: Maximization of Density and Tensile Strength of Laser-Melted Ti6Al-4V Alloy Specimens

The optimization problem examined here is formulated by considering the experimental results presented in [38], where a Taguchi experimental design was established, with the laser power  $LP$  (W), scanning speed  $SS$  (mm/min), hatch spacing  $HS$  ( $\mu\text{m}$ ), scan pattern angle  $SPA$  ( $^\circ$ ) and heat treatment temperature  $HTT$  ( $^\circ\text{C}$ ) being the independent process parameters, to characterize the Brinell hardness  $HB$  (HB) and tensile strength  $TS$  (MPa) of the laser-melted Ti6Al4V alloy specimens. The experimental design involved a total of 25 runs based on the number of parameters and their corresponding levels. The SLM equipment that was used was an SLM-125HL equipped with YLR-fiber-laser with a minimum spot size of  $5\mu\text{m}$ , while the material used was a powdered Ti6Al4V Titanium

alloy. The authors of [38] measured the hardness of their experimental specimens using a DuraJet<sup>®</sup> G5 apparatus for the Brinell hardness. The load and indenter values that were applied were 30 N and 1/30, respectively. The regression equations found in [38] were adopted to play the role of objective functions for the MOVEGA and the rest of the algorithms. The scanning strategy was kept constant. The ranges for the parameters were: ( $90 \leq LP \leq 110$ ), ( $600 \leq SS \leq 800$ ), ( $65 \leq HS \leq 85$ ), ( $36 \leq SPA \leq 75$ ) and ( $20 \leq HTT \leq 1050$ ). Equations (11) and (12) give the regression equations that were used as objective functions for simultaneously maximizing the hardness  $\max HB$  and the tensile strength  $\max TS$  in this two-objective optimization case.

$$\begin{aligned} \max HB = & -(10376 - 152.9 * LP - 4.20 * SS - 52.2 * HS + 43.3 * SPA + 0.336 * HTT + 0.638 * LP^2 + 0.00264 * \\ & SS^2 + 0.204 * HS^2 + 0.0471 * SPA^2 - 0.000091 * HTT^2 + 0.0059 * LP * SS + 0.376 * LP * HS - 0.114 * LP * SPA - \\ & 0.00499 * LP * HTT - 0.00844 * SS * SPA + 0.000486 * SS * HTT - 0.376 * HS * SPA + 0.00175 * HS * HTT - \\ & 0.00465 * SPA * HTT) \end{aligned} \quad (11)$$

$$\begin{aligned} \max TS = & -(-11916 + 389 * LP + 1.3 * SS - 240 * HS + 92 * SPA + 4.23 * HTT - 1.93 * LP^2 + 0.00276 * SS^2 + \\ & 1.443 * HS^2 + 0.549 * SPA^2 - 0.000429 * HTT^2 - 0.0161 * LP * SS + 0.51 * LP * HS - 1.077 * LP * SPA - 0.0003 * LP \\ & * HTT - 0.0272 * SS * SPA - 0.00316 * SS * x(5) - 0.362 * HS * SPA - 0.0225 * HS * HTT + 0.0034 * SPA * HTT) \end{aligned} \quad (12)$$

The two-objective optimization problem was solved by applying the MOVEGA, MOGWO, MOMVO, MOALO and MODA algorithms using a population size that was equal to 20 for 200 iterations (4000 function evaluations). To examine the efficiency of the MOVEGA and the rest of antagonizing algorithms, 30 independent algorithmic simulations were conducted, resulting in 30 non-dominated Pareto fronts. From these 30 sets, the coverage has been computed among the pairs of two independent sets per two algorithms, while the spacing refers to the best non-dominated set obtained out of 30 trials. The standard deviation results refer to the 30 coverage results computed for the five multi-objective optimization algorithms. Figure 5 presents the best Pareto fronts obtained by the algorithms. Table 1 summarizes the results for the best 145 non-dominated solutions set obtained by the MOVEGA, whilst Table 2 gives the results for best results, the mean and the standard deviation for coverage values, as well as the spacing among the solutions for the best non-dominated set obtained by each algorithm. It is evident that the MOVEGA exhibited the best performance in terms of the metrics selected. As an example, the result of  $Cvg(MOVEGA, MOGWO) = 0.8328$  implies that, with reference to the best values, 83.28% of MOGWO's non-dominated solutions are dominated by those obtained by MOVEGA. On the contrary, the result of  $Cvg(MOGWO, MOVEGA) = 0.7213$  implies that, with reference to the best values, 72.13% of MOVEGA's non-dominated solutions are dominated by those obtained by MOGWO. With the same philosophy, the rest of the outputs for the coverage indicator can be similarly interpreted. The best results for the spacing indicator are 0.0257, 0.0912, 0.0922, 0.0697 and 0.0984 for the MOVEGA, MOGWO, MOMVO, MOALO and MODA optimizers, respectively. By considering all three statistical parameters (the best results, the mean and the St.Dev.), MOVEGA is superior to the rest algorithms. By reviewing the Pareto fronts given in Figure 5, it is evident that MOVEGA's Pareto front is more well-spread and continuous, with its 145 non-dominated points being uniformly distributed throughout the entire trend curve.

**Table 1.** Optimal non-dominated solutions set obtained by MOVEGA using the regression equations of case 2.

Sol. No.	LP (W)	SS (mm/min)	HS ( $\mu\text{m}$ )	SPA ( $^\circ$ )	HTT ( $^\circ\text{C}$ )	$\max HB$	$\max TS$
1	90.0000	600.0070	65.0000	74.9992	96.0606	724.1530	1676.6300
2	90.0000	600.0830	65.0000	75.0000	189.6659	716.3600	1768.1500
3	90.0002	600.8099	65.0002	74.9999	369.0359	696.4140	1922.2800
4	90.0004	600.2490	65.0015	74.9992	512.6129	677.2990	2025.6600

Table 1. Cont.

Sol. No.	LP (W)	SS (mm/min)	HS ( $\mu\text{m}$ )	SPA ( $^{\circ}$ )	HTT ( $^{\circ}\text{C}$ )	maxHB	maxTS
5	90.0004	600.0346	65.0005	74.9990	572.3014	668.2410	2063.6400
6	90.0004	600.0497	65.0005	74.9991	572.4180	668.2090	2063.7000
7	90.0002	600.0021	65.0014	74.9992	638.1319	657.2870	2101.8300
8	90.0002	600.0349	65.0013	74.9995	687.7818	648.4690	2128.1600
9	90.0013	600.4803	65.0001	74.9994	74.0921	725.1940	1654.4900
10	90.0020	600.1857	65.0008	74.9994	115.8210	722.4130	1696.6500
11	90.0001	600.7364	65.0004	74.9993	213.9841	713.4070	1790.9200
12	90.0002	600.0025	65.0002	74.9973	48.2313	727.4620	1626.9200
13	90.0001	600.0005	65.0009	74.9910	100.7152	723.7120	1681.0100
14	90.0002	600.0005	65.0009	74.9910	111.3896	722.9010	1691.7700
15	90.0007	600.0103	65.0001	74.9973	322.8056	702.6660	1885.1000
16	90.0003	600.0176	65.0007	74.9885	436.4406	688.3110	1972.6600
17	90.0006	600.0850	65.0001	74.9961	537.9085	673.5970	2042.0900
18	90.0010	600.0852	65.0000	74.9962	575.7634	667.6140	2065.6100
19	90.0037	600.0031	65.0004	74.9998	662.0168	653.0600	2114.7800
20	90.0001	600.0041	65.0001	74.9997	704.9853	645.3690	2136.8900
21	90.0002	600.0046	65.0001	74.9994	740.2719	638.7320	2153.8000
22	90.0055	600.0059	65.0003	74.9959	825.6876	621.5840	2190.0900
23	90.0030	600.0004	65.0006	74.9958	883.3804	609.4070	2211.2500
24	90.0001	600.0022	65.0018	74.9999	959.8236	592.3350	2235.0000
25	90.0000	600.0024	65.0009	74.9995	1049.9481	570.7760	2256.4100
26	90.0009	600.0032	65.0008	74.9997	72.2267	725.8430	1652.1300
27	90.0000	600.1076	65.0023	75.0000	211.0341	714.3050	1787.8900
28	90.0000	600.0121	65.0004	74.9986	300.1269	705.2500	1866.2800
29	90.0000	600.0203	65.0004	74.9984	304.2338	704.7820	1869.7200
30	90.0000	600.0722	65.0004	74.9967	362.5610	697.8850	1917.1000
31	90.0000	600.0714	65.0004	74.9970	362.6760	697.8740	1917.2000
32	90.0000	600.0657	65.0001	74.9993	423.4337	690.1280	1963.6000
33	90.0000	600.0660	65.0002	74.9993	431.3230	689.0670	1969.3800
34	90.0005	600.1135	65.0005	74.9996	482.8846	681.8100	2005.8100
35	90.0005	600.1110	65.0007	74.9997	531.7765	674.5350	2038.2600
36	90.0009	600.0268	65.0031	75.0000	608.8342	662.2050	2085.2100
37	90.0004	600.1641	65.0076	74.9999	689.8788	647.8650	2128.7900
38	90.0007	600.1651	65.0079	74.9999	710.0763	644.1420	2138.8300
39	90.0003	600.0472	65.0192	75.0000	811.1128	624.3400	2183.5100
40	90.0006	600.0391	65.0091	74.9999	875.5373	611.0010	2208.2300
41	90.0001	600.0028	65.0100	74.9999	936.3248	597.5660	2227.8300
42	90.0000	600.0027	65.0050	74.9998	1001.2611	582.5420	2245.5100
43	90.0043	600.0114	65.0043	74.9999	81.6854	725.0330	1661.7300
44	90.0002	600.0909	65.0436	74.9995	353.1494	698.1930	1907.9500
45	90.0002	600.0898	65.0461	74.9995	354.1915	698.0200	1908.6800
46	90.0000	600.0104	65.0133	75.0000	487.6573	680.9800	2008.5600
47	90.0001	600.3778	65.0084	75.0000	552.4658	670.9590	2050.8700
48	90.0003	600.4747	65.0014	74.9992	756.6315	635.1890	2160.6100
49	90.0002	600.4659	65.0014	74.9992	798.6468	626.8870	2178.7200
50	90.0005	600.7370	65.0019	74.9616	860.6133	613.5870	2200.6600
51	90.0000	600.0007	65.0044	74.9999	928.7629	599.3840	2225.8800
52	90.0000	600.0000	65.0019	74.9999	972.2506	589.4500	2238.3600
53	90.0000	600.0231	65.0003	75.0000	1021.0095	577.8650	2250.3200
54	90.0000	600.0224	65.0002	75.0000	1049.6006	570.8650	2256.3600
55	90.0004	600.6827	65.0039	74.9999	280.1177	706.7060	1849.3300
56	90.0000	600.1879	65.0004	74.9928	180.6262	716.9880	1759.4200
57	90.0008	600.1150	65.0002	74.9970	246.9769	710.7680	1820.2900
58	90.0003	600.0007	65.0000	74.9992	20.1417	729.2480	1596.9400

Table 1. Cont.

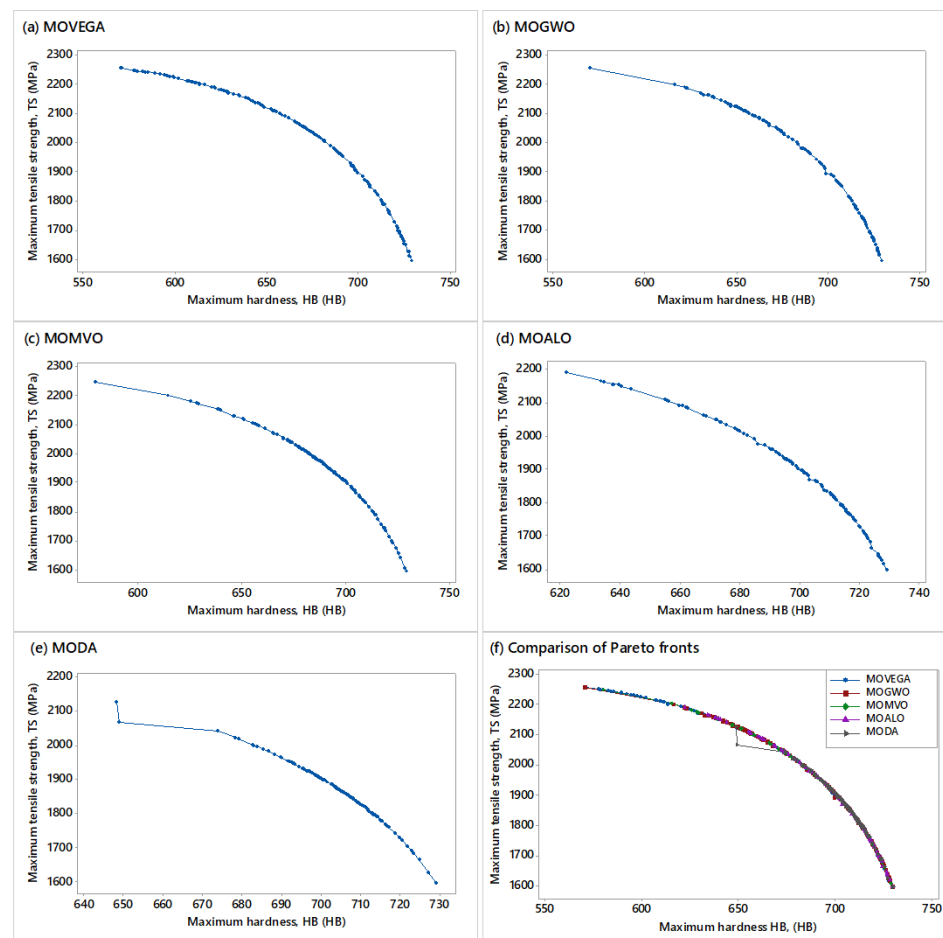
Sol. No.	LP (W)	SS (mm/min)	HS ( $\mu\text{m}$ )	SPA ( $^{\circ}$ )	HTT ( $^{\circ}\text{C}$ )	maxHB	maxTS
59	90.0003	600.0007	65.0001	74.9999	88.6743	724.7030	1669.1200
60	90.0002	600.0009	65.0001	74.9999	115.1837	722.7150	1695.9400
61	90.0001	600.0007	65.0001	74.9999	150.1976	719.8930	1730.4600
62	90.0001	600.0009	65.0001	75.0000	185.7119	716.8010	1764.3900
63	90.0042	600.0007	65.0015	74.9996	229.7076	712.5410	1804.7900
64	90.0005	600.0004	65.0026	74.9996	291.2892	706.1940	1858.7500
65	90.0018	600.0028	65.0023	74.9988	424.0614	690.0180	1963.9300
66	90.0018	600.0004	65.0023	74.9989	436.8278	688.3010	1973.2600
67	90.0075	600.0098	65.0006	74.9999	504.0405	678.6600	2020.0500
68	90.0073	600.0096	65.0004	74.9999	527.3985	675.1570	2035.4100
69	90.0028	600.0066	65.0001	74.9998	580.7397	666.8640	2068.7700
70	90.0031	600.0065	65.0001	74.9998	589.3602	665.4540	2073.9200
71	90.0101	600.0036	65.0005	74.9898	656.1425	653.8770	2111.1400
72	90.0000	600.0052	65.0013	74.9980	718.4244	642.8350	2143.3300
73	90.0000	600.0051	65.0013	74.9980	725.1892	641.5640	2146.5800
74	90.0004	600.0005	65.0003	74.9994	791.4698	628.6960	2176.4300
75	90.0003	600.0001	65.0005	74.9998	806.9547	625.5700	2182.8500
76	90.0009	600.0003	65.0003	74.9981	916.3233	602.2180	2222.1800
77	90.0286	600.0030	65.0050	74.9999	120.2652	721.6730	1700.3900
78	90.0041	600.0147	65.0003	74.9999	192.6370	716.0760	1770.8200
79	90.0041	600.0148	65.0002	74.9999	224.1196	713.1030	1799.8000
80	90.0019	600.0978	65.0022	74.9992	350.5860	699.2630	1907.5900
81	90.0018	600.0980	65.0013	74.9993	377.1215	696.0260	1928.5200
82	90.0010	600.0072	65.0009	75.0000	460.2781	685.1080	1990.1300
83	90.0020	600.0121	65.0008	74.9999	496.3530	679.9050	2014.9700
84	90.0023	600.0167	65.0009	75.0000	562.1374	669.8410	2057.4200
85	90.0002	600.0046	65.0001	74.9985	619.2623	660.5290	2091.2900
86	90.0002	600.0067	65.0000	75.0000	654.6460	654.4410	2110.9200
87	90.0004	600.0434	65.0002	74.9980	760.4103	634.7950	2162.8600
88	90.0006	600.0443	65.0017	74.9988	823.3227	622.1490	2189.2300
89	90.0003	600.0844	65.0009	74.9996	882.0087	609.7240	2210.8200
90	90.0003	600.0177	65.0015	74.9979	943.9839	595.9530	2230.4200
91	90.0002	600.0176	65.0015	74.9979	951.1902	594.3050	2232.4900
92	90.0004	600.0176	65.0004	74.9979	1018.4691	578.4620	2249.6600
93	90.0002	600.0319	65.0009	74.9998	48.8745	727.4000	1627.7000
94	90.0006	600.0274	65.0009	74.9999	101.5424	723.7010	1682.2000
95	90.0006	600.0512	65.0009	74.9998	136.2923	720.9600	1716.8700
96	90.0003	600.0261	65.0000	74.9913	368.4556	697.1580	1921.5300
97	90.0004	600.0854	65.0001	74.9977	443.7262	687.3420	1978.2900
98	90.0006	600.0226	65.0000	74.9978	445.0121	687.2210	1979.2300
99	90.0042	600.0567	65.0008	74.9919	520.7453	676.1180	2030.7800
100	90.0023	600.0569	65.0003	74.9919	526.9859	675.2190	2034.8800
101	90.0165	601.4028	65.0000	74.9997	676.4436	649.0900	2120.7600
102	90.0093	601.0325	65.0000	74.9995	782.6755	629.4820	2171.1900
103	90.0001	600.0025	65.0001	74.9998	891.3549	607.7680	2214.1800
104	90.0001	600.0033	65.0001	74.9998	916.9145	602.1180	2222.4500
105	90.0008	600.1868	65.0000	75.0000	995.3963	583.8910	2243.9900
106	90.0050	600.2147	65.0001	74.9740	36.8009	727.6280	1614.0400
107	90.0354	600.0887	65.0000	75.0000	339.2562	699.9920	1898.0800
108	90.0345	600.1149	65.0000	75.0000	369.8654	696.2760	1922.4300
109	90.0008	600.3937	65.0001	74.9969	543.6894	672.4330	2045.6000
110	90.0001	600.0295	65.0001	74.9962	586.9384	665.8660	2072.3700
111	90.0080	600.8088	65.0015	74.9783	785.2215	628.9980	2171.6700
112	90.0010	600.1271	65.0004	74.9988	874.0360	611.4080	2207.9800

Table 1. Cont.

Sol. No.	LP (W)	SS (mm/min)	HS ( $\mu\text{m}$ )	SPA ( $^{\circ}$ )	HTT ( $^{\circ}\text{C}$ )	maxHB	maxTS
113	90.0007	600.1159	65.0004	74.9988	893.1665	607.2660	2214.5200
114	90.0016	600.0141	65.0000	74.9992	988.4006	585.6400	2242.5500
115	90.0000	600.0025	65.0008	74.9991	20.3040	729.2250	1597.0900
116	90.0000	600.0005	65.0008	74.9991	33.4874	728.4180	1611.2800
117	90.0002	600.0437	65.0000	74.9975	130.6390	721.4280	1711.2500
118	90.0002	600.0452	65.0000	74.9968	255.4522	709.9870	1827.7600
119	90.0004	600.6115	65.0009	75.0000	310.5811	703.4860	1875.1500
120	90.0001	600.0099	65.0000	74.9991	412.8274	691.5840	1955.7500
121	90.0000	600.0305	65.0000	74.9945	486.1262	681.3920	2007.8800
122	90.0000	600.0510	65.0000	74.9944	519.8299	676.3860	2030.3800
123	90.0002	600.1056	65.0001	74.9994	629.5712	658.6990	2097.0500
124	90.0004	600.0521	65.0002	74.9998	698.4567	646.5270	2133.5900
125	90.0001	600.0234	65.0010	74.9995	774.9020	631.9700	2169.3000
126	90.0001	600.0352	65.0021	74.9992	793.4223	628.2500	2177.1100
127	90.0008	600.2279	65.0000	74.9988	831.5273	620.3430	2192.2400
128	90.0008	600.2258	65.0000	74.9988	850.5332	616.3640	2199.4100
129	90.0073	600.0691	65.0014	74.9974	1011.2398	579.9870	2247.7200
130	90.0011	600.0000	65.0001	74.9997	33.3880	728.4230	1611.2000
131	90.0015	600.0003	65.0000	74.9999	99.9996	723.8460	1680.6300
132	90.0011	600.0006	65.0000	74.9935	175.7097	717.6130	1754.6800
133	90.0001	600.0113	65.0002	74.9997	228.5262	712.7510	1803.8400
134	90.0004	600.0113	65.0002	74.9999	263.4553	709.2120	1834.8800
135	90.0003	600.0115	65.0002	74.9999	287.0514	706.6990	1855.2500
136	90.0012	600.0139	65.0001	74.9987	418.1687	690.8460	1959.6800
137	90.0008	600.0165	65.0001	74.9994	450.2061	686.5170	1983.0000
138	90.0026	600.0003	65.0029	74.9998	524.5331	675.6510	2033.5100
139	90.0017	600.0001	65.0004	74.9954	648.2606	655.4900	2107.2500
140	90.0005	600.0005	65.0011	74.9997	699.6744	646.3240	2134.2100
141	90.0005	600.0005	65.0017	74.9997	733.9239	639.9090	2150.7700
142	90.0097	600.0000	65.0000	74.9954	788.8330	628.9920	2175.0300
143	90.0099	600.0009	65.0001	74.9954	863.4788	613.5420	2204.1900
144	90.0099	600.0009	65.0001	74.9954	864.0086	613.4290	2204.3800
145	90.0119	600.0029	65.0002	74.9701	926.9109	599.4130	2224.1300

Table 2. Best, mean and standard deviation results for the non-dominated solutions obtained by MOVEGA, MOGWO, MOMVO, MOALO and MODA optimizers for case 2.

Performance Metric	Statistical Results		
	Best	Mean	St.Dev.
Cvg(MOVEGA, MOGWO)	0.8328	0.7641	0.0442
Cvg(MOGWO, MOVEGA)	0.7213	0.0912	0.0753
Cvg(MOVEGA, MOMVO)	0.8412	0.7327	0.0548
Cvg(MOMVO, MOVEGA)	0.2674	0.1668	0.0349
Cvg(MOVEGA, MOALO)	0.8227	0.7808	0.0648
Cvg(MOALO, MOVEGA)	0.2942	0.2105	0.0599
Cvg(MOVEGA, MODA)	0.7828	0.3571	0.0642
Cvg(MODA, MOVEGA)	0.2118	0.2942	0.0341
S(MOVEGA)	0.0257	0.0274	0.0035
S(MOGWO)	0.0912	0.1077	0.0094
S(MOVMVO)	0.0922	0.1752	0.0104
S(MOALO)	0.0697	0.1777	0.0149
S(MODA)	0.0984	0.2101	0.0211



**Figure 5.** Pareto fronts for the non-dominated solutions obtained from the best simulation experiment exhibited by: (a) MOVEGA, (b) MOGWO, (c) MOMVO, (d) MOALO, (e) MODA and (f) Comparison of Pareto fronts algorithms for case 2, with 20 individuals and 200 iterations.

#### 4.3. Case 3: Three-Objective Optimization Problem for 316 L Stainless Steel Powder Bed Fusion Operation

The optimization problem examined in this case is formulated by considering the experimental results presented in [39]. In [39], a Taguchi experimental design was established, with the laser power  $LP$  (W), scanning speed  $SS$  ( $\text{mm s}^{-1}$ ), and hatch spacing  $HS$  (mm) being the independent process parameters, to characterize the top surface roughness  $Ra$  ( $\mu\text{m}$ ), Vickers hardness  $HV$  (HV) and density in percentage  $\rho$  (%) of laser-melted 316 L stainless steel specimens. Their experimental design involved a total of 27 runs based on the number of parameters and their corresponding levels. The SLM equipment used was the EP250 with a fiber-laser with 400 W maximum indicative power and 80  $\mu\text{m}$  beam diameter. The oxygen content was maintained at approximately 1000 ppm during the conduction of SLM experiments. The results corresponding to the three objectives, the top surface roughness  $Ra$  ( $\mu\text{m}$ ), Vickers hardness  $HV$  (HV) and density in percentage  $\rho$  (%), were the average values as a result of taking series of measurements. The authors of [39] succeeded on presenting a factor analysis, which was accompanied by normalized quantities along with the Taguchi design of the experiments, however, the kind of trade-off these objectives yielded and the type of solution space in the form of a Pareto front were not discussed. The regression equations found in [39] were adopted to serve as the objective functions for the MOVEGA and the rest algorithms for the simultaneous optimization efforts of the three objectives. From these objectives, one of them should be minimized (top surface roughness  $Ra$ ) and two of them should be maximized (Vickers hardness  $HV$  and density in percentage,  $\rho$ ). The ranges for the parameters were: ( $44.36 \leq LP \leq 64.17$ ), ( $6.69 \leq SS \leq 9.67$ )

and  $(1.88 \leq HS \leq 2.63)$ . Equations (13) and (15) give the regression equations that were used as objective functions for simultaneously minimizing the surface roughness  $\min Ra$ , maximizing the Vickers hardness  $\max HV$  and the maximizing density in percentage  $\max \rho$  in this three-objective optimization case.

$$\min Ra = 21.3 - 1.735 * LP + 3.10 * SS + 21.8 * HS + 0.00811 * LP^2 - 0.261 * SS^2 - 3.65 * HS^2 + 0.0610 * LP * SS + 0.051 * LP * HS - 0.782 * SS * HS \tag{13}$$

$$\max HV = -(-206 + 0.73 * LP + 38.8 * SS + 234 * HS - 0.1111 * LP^2 - 3.62 * SS^2 - 61.6 * HS^2 + 0.836 * LP * SS + 2.40 * LP * HS - 13.57 * SS * HS) \tag{14}$$

$$\max \rho = -(94.76 - 0.0235 * LP + 0.553 * SS + 3.29 * HS - 0.002043 * LP^2 - 0.0505 * SS^2 - 0.761 * HS^2 + 0.01875 * LP * SS + 0.0530 * LP * HS - 0.4188 * SS * HS) \tag{15}$$

In this case, the algorithms ran for 4000 function evaluations using a population size that was equal to 20 for 200 iterations, whilst 50 non-dominated solutions were stored in corresponding archives. To examine the efficiency of the MOVEGA and the rest of antagonizing algorithms, 30 independent algorithmic simulations were conducted, resulting in 30 non-dominated Pareto fronts. From these 30 sets, the coverage was computed among the pairs of two independent sets per two algorithms, while the spacing refers to the best non-dominated set obtained out of 30 trials. The standard deviation results refer to the thirty coverage results computed for the five multi-objective optimization algorithms. Figure 6 illustrates the best Pareto fronts obtained by the algorithms.

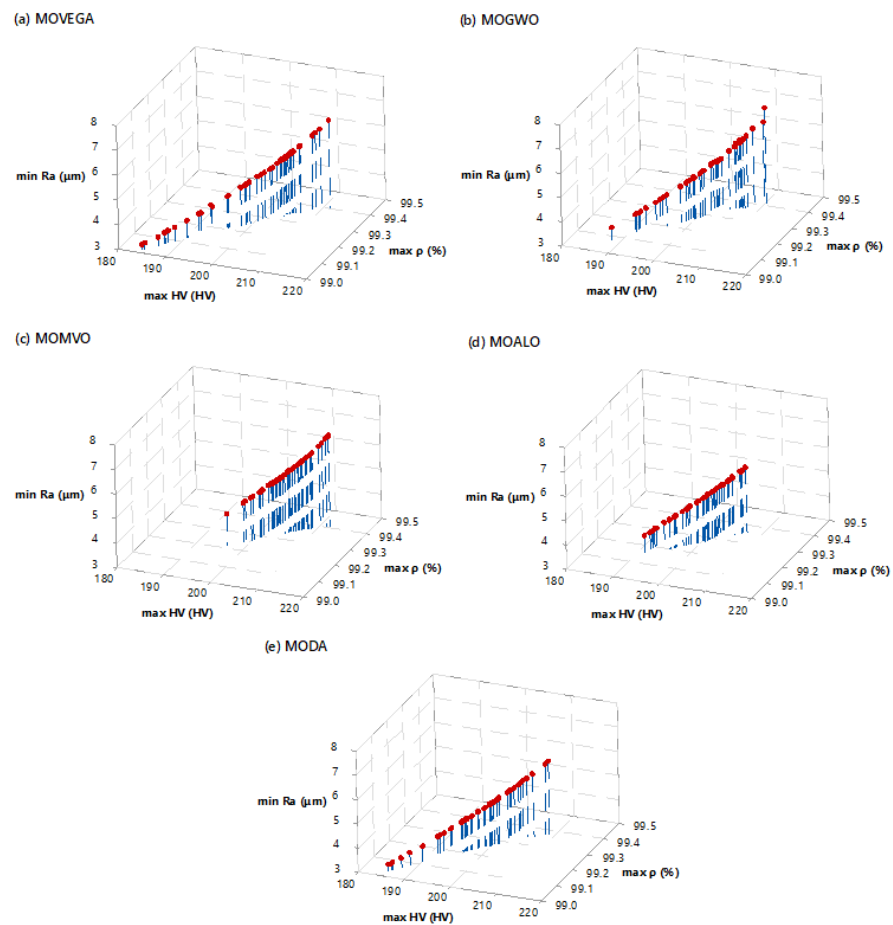


**Figure 6.** Pareto fronts of non-dominated solutions for the best simulation experiment exhibited by: (a) MOVEGA, (b) MOGWO, (c) MOMVO, (d) MOALO and (e) MODA algorithms for case 3, with 20 individuals and 200 iterations.



Table 3 summarizes the results for the best 145 non-dominated solutions set obtained by the MOVEGA, whilst Table 4 gives the results for best results, and the mean and the standard deviation for the coverage values, as well as spacing among the solutions for the best non-dominated set obtained by each algorithm. It is revealed that the MOVEGA exhibited the best performance in terms of the metrics selected. As an example, the result of  $Cvg(MOVEGA, MOGWO) = 0.8745$  implies that, with reference to the best values, 87.45% of MOGWO's non-dominated solutions are dominated by those obtained by MOVEGA. On the contrary, the result of  $Cvg(MOGWO, MOVEGA) = 0.4249$  implies that, with reference to the best values, 42.49% of MOVEGA's non-dominated solutions are dominated by those obtained by MOGWO. Similarly, the rest of the outputs referring to the coverage indicator were interpreted. The best results for the spacing indicator are 0.0177, 0.0181, 0.0102, 0.0125 and 0.0184 for the MOVEGA, MOGWO, MOMVO, MOALO and MODA optimizers, respectively. Note that MOMVO and MOALO achieved the best spacing results, however, their solution sets are poorer compared to the rest algorithm results. That is, MOVEGA's non-dominated solutions offer a wider range for selecting optimal solutions according to the operation's requirements. By reviewing the Pareto fronts given in Figure 6, it is evident that MOVEGA's front is spread more, continuous and wider than the others, with its 50 non-dominated points being uniformly distributed throughout the entire trend curve.

**Table 3.** Optimal non-dominated solutions set obtained by MOVEGA by applying the regression equations of case 3.

Sol. No.	LP (W)	SS (mm/min)	HS ( $\mu\text{m}$ )	minRa	maxHV	max $\rho$
1	63.0920	6.6900	1.8800	3.22026	184.430	99.0131
2	57.0923	7.0746	2.0314	6.08493	208.998	99.3881
3	56.5919	7.2272	2.0667	6.55576	211.269	99.4072
4	63.3478	6.7351	1.8882	3.30673	184.917	99.0189
5	59.7448	6.6900	1.8800	4.00626	193.844	99.1784
6	57.6960	6.8654	1.9544	5.26003	203.770	99.3269
7	59.0302	7.0065	2.0128	5.40195	205.081	99.3343
8	59.6797	6.7893	1.8937	4.27655	196.154	99.2116
9	57.5663	7.0654	1.9750	5.68598	206.682	99.3604
10	57.4215	7.0615	2.0316	5.97916	208.501	99.3817
11	60.6645	6.7139	1.8846	3.84318	192.136	99.1468
12	62.3797	6.6900	1.8800	3.37229	186.642	99.0521
13	62.3644	6.7182	1.8866	3.46950	187.562	99.0662
14	58.7394	6.9052	1.9771	5.15238	203.262	99.3139
15	58.4793	7.0090	1.9913	5.44380	205.308	99.3399
16	62.3863	6.7290	1.8862	3.48354	187.657	99.0675
17	58.4011	6.9702	1.9761	5.33356	204.510	99.3308
18	58.6260	6.7573	1.9064	4.57371	198.665	99.2541
19	60.9559	6.8512	1.9448	4.35574	196.533	99.2082
20	61.2156	6.7024	1.8862	3.69831	190.570	99.1197
21	61.8754	6.7370	1.8812	3.58157	188.985	99.0912
22	60.6341	6.7259	1.8868	3.88524	192.521	99.1526
23	58.8913	6.8463	1.9457	4.86012	201.031	99.2839
24	60.6267	6.8324	1.9279	4.30814	196.244	99.2062
25	58.4646	6.9468	1.9886	5.34328	204.607	99.3322
26	58.1004	6.9805	1.9960	5.52379	205.786	99.3483
27	59.5401	6.9638	1.9837	5.07353	202.676	99.3008
28	59.6232	6.9664	1.9792	5.03499	202.370	99.2962
29	58.2348	6.9789	1.9901	5.45795	205.362	99.3423
30	59.2099	6.9712	1.9831	5.16324	203.357	99.3115
31	59.5973	6.9073	1.9500	4.80039	200.538	99.2722
32	58.3600	6.9500	1.9838	5.35188	204.644	99.3331

Table 3. Cont.

Sol. No.	LP (W)	SS (mm/min)	HS ( $\mu\text{m}$ )	minRa	maxHV	max $\rho$
33	59.5956	6.8831	1.9562	4.79400	200.511	99.2722
34	58.2513	6.9896	1.9909	5.47262	205.466	99.3434
35	57.0567	7.1305	2.0458	6.22802	209.792	99.3950
36	60.6599	6.8332	1.9296	4.31110	196.260	99.2062
37	58.2678	6.9376	1.9778	5.32860	204.455	99.3314
38	60.4834	6.9424	1.9605	4.69952	199.536	99.2528
39	59.2840	7.0080	1.9910	5.23907	203.907	99.3178
40	61.9641	6.7711	1.9043	3.76112	190.613	99.1149
41	60.5560	6.8732	1.9534	4.53106	198.169	99.2338
42	59.5237	6.9291	1.9660	4.93497	201.613	99.2871
43	61.6147	6.8326	1.9338	4.11536	194.069	99.1683
44	59.0104	6.9904	1.9925	5.28737	204.261	99.3241
45	61.5612	6.8335	1.9305	4.11072	194.054	99.1684
46	60.1161	6.8770	1.9438	4.59124	198.773	99.2449
47	62.7393	6.7634	1.9016	3.56492	188.083	99.0715
48	60.7520	6.8414	1.9321	4.31713	196.273	99.2057
49	60.5726	6.9424	1.9639	4.69620	199.484	99.2515
50	58.3231	7.0466	2.0144	5.64501	206.650	99.3565

Table 4. Best, mean and standard deviation results for the non-dominated solutions obtained by MOVEGA, MOGWO, MOMVO, MOALO and MODA optimizers for case 3.

Performance Metric	Statistical Results		
	Best	Mean	St.Dev.
Cvg(MOVEGA, MOGWO)	0.8745	0.8524	0.0346
Cvg(MOGWO, MOVEGA)	0.4249	0.4390	0.0571
Cvg(MOVEGA, MOMVO)	0.4612	0.4588	0.0224
Cvg(MOMVO, MOVEGA)	0.2459	0.2547	0.0489
Cvg(MOVEGA, MOALO)	0.4378	0.4174	0.0542
Cvg(MOALO, MOVEGA)	0.1947	0.2234	0.0672
Cvg(MOVEGA, MODA)	0.7716	0.7519	0.0516
Cvg(MODA, MOVEGA)	0.6904	0.6815	0.0672
S(MOVEGA)	0.0177	0.0179	0.0031
S(MOGWO)	0.0181	0.0186	0.0046
S(MOVMVO)	0.0102	0.0111	0.0012
S(MOALO)	0.0125	0.0128	0.0018
S(MODA)	0.0184	0.0178	0.0057

## 5. Conclusions

In this research, a modified virus-evolutionary genetic algorithm for single and multi-objective optimization problems has been presented. The algorithm takes advantage of two populations; one comprising the main individuals and the other one comprising the population of viruses. Owing to the fact that the physical process of viral infection has been simulated in this algorithm, both the horizontal propagation and vertical inheritance operators are responsible for obtaining more reliable and antagonizing solutions compared to those results obtained by the other algorithms. Through their coevolution, the individuals and viruses exchange information to push further the envelope of maintaining the balance between exploitation and exploration, while efficient binary schemata are rapidly processed, and if they are beneficial, they increase the algorithm's efficiency in finding either the global optimum for single-objective optimization problems or a uniform and wide non-dominated set of solutions for multi-objective optimization problems.

The algorithm has been applied for solving three optimization problems related to a modern additive manufacturing/rapid prototyping operation, which is widely known as selective laser sintering and/or selective laser melting (SLS/SLM). The first case presented a single-objective optimization problem using the maximum density as its optimization target when laser-melting Ti6Al4V alloy powder was used for fabricating parts. The second case presented a bi-objective optimization problem using the maximum hardness and maximum tensile strength as the optimization objectives for simultaneous optimization when laser-melting Ti6Al4V alloy powder was used for fabricating parts. The third case presented a three-objective optimization problem, where a simultaneous optimization among the minimum surface roughness, maximum hardness and maximum density needed to be achieved during the laser melting of 316 L stainless steel. All three cases have been adopted by the recent literature, and the regression equations from corresponding experiments have served as the objective functions for the problems.

By applying five different optimization algorithms, including the one proposed in this work (virus-evolutionary genetic algorithm), it was shown that a significant trade-off among the objectives of the several cases exists, and it constitutes an important research aspect for optimizing engineering applications using intelligent algorithms. The rest of the algorithms tested were the Greywolf (MOGWO), the Multi-verse (MOMVO), the Antlion (MOALO) and the dragonfly algorithms (MODA). The results obtained by the three aforementioned cases examined in the work have been rigorously compared under the same conditions to the best possible extent since all the algorithms handle the same population size, number of iterations, number of function evaluations and initialization conditions with the same starting search points. To characterize the performance of the proposed virus-evolutionary genetic algorithm as well as the rest of competitive algorithms, two widely applied performance indicators have been computed; the coverage between the two non-dominated solution sets and spacing used to quantify the solutions spread.

It should be mentioned that the application of the virus-evolutionary genetic algorithm to the individual cases examined in our current study by no means constitutes a generalized optimization methodology dedicated to SLS/SLM operations. The results presented in this study are as reliable as the problems' domains and their related parameters will allow them to be. However, this work, in its current state, puts forth new knowledge by developing and enhancing the virus-evolutionary genetic algorithm for efficiently searching several problem domains in real-world experiments. By taking into account the great number of similar studies that have attempted to acquire results with commonly employed artificial algorithms, this work has embraced "viral infectivity" to come up with original datasets and results related to SLS/SLM operation to allow comparisons to be made with other research by applying other heuristics. The benefits of the proposed optimization algorithm against other competitive algorithms is the computational philosophy of the algorithm based on the virus theory of evolution. The viruses in this algorithm act as "hill-climbers" and manage to lead the search for the solution so that local trapping is avoided. The rest of competitive algorithms are also beneficial, and their control environment has a low cost, is user friendly and requires a basic technical computing level (i.e., in the MATLAB environment). The limitation of the proposed methodology is that no online monitoring for the direct control of process parameters and optimization is necessary. The current trends suggest that we need new technology for optimizing the process parameters by analyzing the signals and suitably balancing the operational parameters to reach an optimal solution.

It is within our interests in the near future to examine the potentials of automating the software that controls the SLS/SLM parameters and try to develop a dynamic optimization environment by using the proposed virus-evolutionary genetic algorithm, which operates in-line with an application program interface of SLS/SLM software, which we envision will be a more meaningful and generic path towards delivering a generalized global optimization solution to further advance scientific knowledge and contribute to engineering optimization.

**Author Contributions:** Conceptualization, N.A.F., J.D.K. and N.M.V.; methodology, N.A.F.; software, N.A.F.; validation, N.A.F. and J.D.K.; formal analysis, N.A.F.; investigation, N.A.F.; resources, N.A.F. and N.M.V.; data curation, N.A.F., J.D.K. and N.M.V.; writing—original draft preparation, N.A.F.; writing—review and editing, N.A.F. and J.D.K.; visualization, N.M.V.; supervision, N.M.V.; project administration, J.D.K. and N.M.V. All authors have read and agreed to the published version of the manuscript.

**Funding:** This research received no external funding.

**Institutional Review Board Statement:** Not applicable.

**Informed Consent Statement:** Not applicable.

**Data Availability Statement:** Not applicable.

**Conflicts of Interest:** The authors declare no conflict of interest.

## References

1. Fashanu, O.; Buchely, M.F.; Spratt, M.; Newkirk, J.; Chandrashekhara, K.; Misak, H.; Walker, M. Effect of SLM Build Parameters on the Compressive Properties of 304L Stainless Steel. *J. Manuf. Mater. Process.* **2019**, *3*, 43. [\[CrossRef\]](#)
2. Maurya, H.S.; Kollo, L.; Tarraste, M.; Juhani, K.; Sergejev, F.; Prashanth, K.G. Effect of the Laser Processing Parameters on the Selective Laser Melting of TiC–Fe–Based Cermets. *J. Manuf. Mater. Process.* **2022**, *6*, 35. [\[CrossRef\]](#)
3. Impey, S.; Saxena, P.; Salonitis, K. Selective Laser Sintering Induced Residual Stresses: Precision Measurement and Prediction. *J. Manuf. Mater. Process.* **2021**, *5*, 101. [\[CrossRef\]](#)
4. Mahardika, M.; Setyawan, M.A.; Sriani, T.; Miki, N.; Prihandana, G.S. Electropolishing Parametric Optimization of Surface Quality for the Fabrication of a Titanium Microchannel Using the Taguchi Method. *Machines* **2021**, *9*, 325. [\[CrossRef\]](#)
5. Zolfpour-Arokhlo, M.; Selamat, A.; Mohd Hashim, S.Z.; Afkhami, H. Modeling of Route Planning System Based on Q Value-Based Dynamic Programming with Multi-Agent Reinforcement Learning Algorithms. *Eng. Appl. Artif. Intell.* **2014**, *29*, 163–177. [\[CrossRef\]](#)
6. Liang, R.; Chen, Y.; Zhu, R. A Novel Fault Diagnosis Method Based on the KELM Optimized by Whale Optimization Algorithm. *Machines* **2022**, *10*, 93. [\[CrossRef\]](#)
7. Tyagi, S.K.; Yang, K.; Tyagi, A.; Dwivedi, S.N. Development of a Fuzzy Goal Programming Model for Optimization of Lead Time and Cost in an Overlapped Product Development Project Using a Gaussian Adaptive Particle Swarm Optimization-Based Approach. *Eng. Appl. Artif. Intell.* **2011**, *24*, 866–879. [\[CrossRef\]](#)
8. Li, S.; Mu, N.; Le, J.; Liao, X. A Novel Algorithm for Privacy Preserving Utility Mining Based on Integer Linear Programming. *Eng. Appl. Artif. Intell.* **2019**, *81*, 300–312. [\[CrossRef\]](#)
9. Gong, K.; Chen, C. Multiple-Attribute Decision Making Based on Equivalence Consistency under Probabilistic Linguistic Dual Hesitant Fuzzy Environment. *Eng. Appl. Artif. Intell.* **2019**, *85*, 393–401. [\[CrossRef\]](#)
10. Chakraborty, S.; Mitra, A. Parametric Optimization of Abrasive Water-Jet Machining Processes Using Grey Wolf Optimizer. *Mater. Manuf. Process.* **2018**, *33*, 1471–1482. [\[CrossRef\]](#)
11. Pawar, P.J.; Rao, R.V. Parameter Optimization of Machining Processes Using Teaching–Learning–Based Optimization Algorithm. *Int. J. Adv. Manuf. Technol.* **2013**, *67*, 995–1006. [\[CrossRef\]](#)
12. Mirjalili, S.; Saremi, S.; Mirjalili, S.M.; Coelho, L.D.S. Multi-Objective Grey Wolf Optimizer: A Novel Algorithm for Multi-Criterion Optimization. *Expert Syst. Appl.* **2016**, *47*, 106–119. [\[CrossRef\]](#)
13. Yue, Z.; Huang, C.; Zhu, H.; Wang, J.; Yao, P.; Liu, Z. Optimization of Machining Parameters in the Abrasive Waterjet Turning of Alumina Ceramic Based on the Response Surface Methodology. *Int. J. Adv. Manuf. Technol.* **2014**, *71*, 2107–2114. [\[CrossRef\]](#)
14. Venkata Rao, R.; Kalyankar, V.D. Parameter Optimization of Modern Machining Processes Using Teaching–Learning–Based Optimization Algorithm. *Eng. Appl. Artif. Intell.* **2013**, *26*, 524–531. [\[CrossRef\]](#)
15. Rao, R.V.; Rai, D.P. Optimization of Fused Deposition Modeling Process Using Teaching–Learning–Based Optimization Algorithm. *Eng. Sci. Technol. Int. J.* **2016**, *19*, 587–603. [\[CrossRef\]](#)
16. Sood, A.K.; Equbal, A.; Toppo, V.; Ohdar, R.K.; Mahapatra, S.S. An Investigation on Sliding Wear of FDM Built Parts. *CIRP J. Manuf. Sci. Technol.* **2012**, *5*, 48–54. [\[CrossRef\]](#)
17. Sood, A.K.; Ohdar, R.K.; Mahapatra, S.S. Experimental Investigation and Empirical Modelling of FDM Process for Compressive Strength Improvement. *J. Adv. Res.* **2012**, *3*, 81–90. [\[CrossRef\]](#)
18. Peng, A.; Xiao, X.; Yue, R. Process Parameter Optimization for Fused Deposition Modeling Using Response Surface Methodology Combined with Fuzzy Inference System. *Int. J. Adv. Manuf. Technol.* **2014**, *73*, 87–100. [\[CrossRef\]](#)
19. Gurralla, P.K.; Regalla, S.P. Multi-Objective Optimisation of Strength and Volumetric Shrinkage of FDM Parts. *Virtual Phys. Prototyp.* **2014**, *9*, 127–138. [\[CrossRef\]](#)
20. Sood, A.K.; Ohdar, R.K.; Mahapatra, S.S. Parametric Appraisal of Mechanical Property of Fused Deposition Modelling Processed Parts. *Mater. Des.* **2010**, *31*, 287–295. [\[CrossRef\]](#)

21. Rao, R.V.; Rai, D.P.; Balic, J. A Multi-Objective Algorithm for Optimization of Modern Machining Processes. *Eng. Appl. Artif. Intell.* **2017**, *61*, 103–125. [[CrossRef](#)]
22. Kuriakose, S.; Shunmugam, M.S. Multi-Objective Optimization of Wire-Electro Discharge Machining Process by Non-Dominated Sorting Genetic Algorithm. *J. Mater. Process. Technol.* **2005**, *170*, 133–141. [[CrossRef](#)]
23. Kumar Pandey, A.; Kumar Dubey, A. Simultaneous Optimization of Multiple Quality Characteristics in Laser Cutting of Titanium Alloy Sheet. *Opt. Laser Technol.* **2012**, *44*, 1858–1865. [[CrossRef](#)]
24. Bhattacharyya, B.; Sorkhel, S.K. Investigation for Controlled Ellectrochemical Machining through Response Surface Methodology-Based Approach. *J. Mater. Process. Technol.* **1999**, *86*, 200–207. [[CrossRef](#)]
25. Bhavsar, S.N.; Aravindan, S.; Rao, P.V. Investigating Material Removal Rate and Surface Roughness Using Multi-Objective Optimization for Focused Ion Beam (FIB) Micro-Milling of Cemented Carbide. *Precis. Eng.* **2015**, *40*, 131–138. [[CrossRef](#)]
26. Rao, R.V.; Rai, D.P.; Balic, J. Multi-Objective Optimization of Machining and Micro-Machining Processes Using Non-Dominated Sorting Teaching–Learning-Based Optimization Algorithm. *J. Intell. Manuf.* **2018**, *29*, 1715–1737. [[CrossRef](#)]
27. Rao, R.V.; Rai, D.P.; Balic, J. Multi-Objective Optimization of Abrasive Waterjet Machining Process Using Jaya Algorithm and PROMETHEE Method. *J. Intell. Manuf.* **2019**, *30*, 2101–2127. [[CrossRef](#)]
28. Kubota, N.; Fukuda, T.; Shimojima, K. Virus-Evolutionary Genetic Algorithm for a Self-Organizing Manufacturing System. *Comput. Ind. Eng.* **1996**, *30*, 1015–1026. [[CrossRef](#)]
29. Lu, B.; Cheng, B. The Virus Evolutionary Genetic Algorithm for Non- Full Loaded Vehicle Scheduling Problem with Fuzzy Time Window. In Proceedings of the 2011 Seventh International Conference on Natural Computation, Shanghai, China, 26–28 July 2011; IEEE: Piscataway, NJ, USA, 2011; pp. 306–310. [[CrossRef](#)]
30. Fountas, N.A.; Benhadj-Djilali, R.; Stergiou, C.I.; Vaxevanidis, N.M. An Integrated Framework for Optimizing Sculptured Surface CNC Tool Paths Based on Direct Software Object Evaluation and Viral Intelligence. *J. Intell. Manuf.* **2019**, *30*, 1581–1599. [[CrossRef](#)]
31. Jakob, W.; Blume, C. Pareto Optimization or Cascaded Weighted Sum: A Comparison of Concepts. *Algorithms* **2014**, *7*, 166–185. [[CrossRef](#)]
32. Anderson, N.G. Evolutionary Significance of Virus Infection. *Nature* **1970**, *227*, 1346–1347. [[CrossRef](#)] [[PubMed](#)]
33. Zitzler, E.; Thiele, L. Multiobjective Evolutionary Algorithms: A Comparative Case Study and the Strength Pareto Approach. *IEEE Trans. Evol. Comput.* **1999**, *3*, 257–271. [[CrossRef](#)]
34. Sun, J.; Yang, Y.; Wang, D. Parametric Optimization of Selective Laser Melting for Forming Ti6Al4V Samples by Taguchi Method. *Opt. Laser Technol.* **2013**, *49*, 118–124. [[CrossRef](#)]
35. Mirjalili, S. Dragonfly Algorithm: A New Meta-Heuristic Optimization Technique for Solving Single-Objective, Discrete, and Multi-Objective Problems. *Neural Comput. Appl.* **2016**, *27*, 1053–1073. [[CrossRef](#)]
36. Mirjalili, S.; Jangir, P.; Saremi, S. Multi-Objective Ant Lion Optimizer: A Multi-Objective Optimization Algorithm for Solving Engineering Problems. *Appl. Intell.* **2017**, *46*, 79–95. [[CrossRef](#)]
37. Mirjalili, S.; Jangir, P.; Mirjalili, S.Z.; Saremi, S.; Trivedi, I.N. Optimization of Problems with Multiple Objectives Using the Multi-Verse Optimization Algorithm. *Knowl.-Based Syst.* **2017**, *134*, 50–71. [[CrossRef](#)]
38. Khorasani, A.; Gibson, I.; Awan, U.S.; Ghaderi, A. The Effect of SLM Process Parameters on Density, Hardness, Tensile Strength and Surface Quality of Ti-6Al-4V. *Addit. Manuf.* **2019**, *25*, 176–186. [[CrossRef](#)]
39. Jiang, H.-Z.; Li, Z.-Y.; Feng, T.; Wu, P.-Y.; Chen, Q.-S.; Feng, Y.-L.; Li, S.-W.; Gao, H.; Xu, H.-J. Factor Analysis of Selective Laser Melting Process Parameters with Normalised Quantities and Taguchi Method. *Opt. Laser Technol.* **2019**, *119*, 105592. [[CrossRef](#)]

**Disclaimer/Publisher’s Note:** The statements, opinions and data contained in all publications are solely those of the individual author(s) and contributor(s) and not of MDPI and/or the editor(s). MDPI and/or the editor(s) disclaim responsibility for any injury to people or property resulting from any ideas, methods, instructions or products referred to in the content.